Journal of Quantitative Spectroscopy & Radiative Transfer 140 (2014) 37–47

Contents lists available at ScienceDirect

Journal of Quantitative Spectroscopy & Radiative Transfer

journal homepage: www.elsevier.com/locate/jqsrt

Spectroscopy and radiation trapping of Yb^{3+} ions in lead phosphate glasses

K. Venkata Krishnaiah [a], R. Rajeswari [a], K. Upendra Kumar [b], S. Surendra Babu [c], I.R. Martín [d], C.K. Jayasankar [a,*]

[a] Department of Physics, Sri Venkateswara University, Tirupati 517502, India
[b] Grupo de Fotônica e Fluidos Complexos, Instituto de Física, Universidade Federal de Alagoas, Maceió-AL 57072-970, Brazil
[c] Directorate of Laser Systems, Research Centre Imarat, Hyderabad 500069, India
[d] Departamento de Física Fundamental y Experimental, Electrónica y Sistemas and MALTA Consolider Team, Universidad de La Laguna, E-38200 San Cristóbal de La Laguna, Santa Cruz de Tenerife, Spain

ARTICLE INFO

Article history:
Received 27 July 2013
Received in revised form
30 January 2014
Accepted 3 February 2014
Available online 10 February 2014

Keywords:
Lead phosphate glasses
Yb^{3+} ions
Near infra-red emission
Radiation trapping
High energy and high power lasers

ABSTRACT

This paper reports ytterbium-doped lead phosphate (PbPhYb) glasses made by melt-quenching technique and their linear and nonlinear refractive indices. Raman and FTIR spectral analysis has been carried out to investigate the functional groups that constitute the host matrix. The oscillator strength of the absorption transition, ($^2F_{7/2} \rightarrow {}^2F_{5/2}$) has been evaluated by using the Smakula model for various concentrations. The near infra-red emission and excitation spectra have been investigated and observed that the profile of the emission spectra changes as a function of Yb_2O_3 concentration, temperature, optical path length and thickness of the sample. From the optical absorption spectra, the spectroscopic and laser performance parameters have been evaluated and in turn used to estimate the gain cross-section of the Yb^{3+} ions. On the other hand, the lifetime for the $^2F_{5/2}$ level of Yb^{3+} ion decreases with increase in Yb_2O_3 concentration up to 6 mol% after an initial increase due to energy migration among the Yb^{3+} ions. The increase in lifetime could be due to radiation trapping but when the concentration is enlarged the energy migration processes are more predominant. The emission profile and lifetime change when the temperature is reduced to cryogenic temperature (11 K). The results reveal that the prepared glasses could be considered for high energy and high power laser as well as solid state cryocooler applications.

1. Introduction

Solid state lasers operating at around the 1.0 μm region are of great interest for many applications such as high resolution spectroscopy, range/gap measurements, material characterization, etc. Trivalent ytterbium (Yb^{3+}) doped laser gain media has received a great deal of interest for 1.0 μm laser under InGaAs laser diode pumping. The large spectral bandwidth of Yb^{3+} ions in glassy hosts, compared with Nd^{3+} ions, permits solid-state laser operation with sub-picosecond pulses [1]. Since Yb^{3+}-doped lasers are quasi three-level systems, higher intensity pumping is required than that of Nd^{3+}-doped lasers, but the thermal effects in Yb^{3+} lasers are negligible as a consequence of a smaller quantum defect. Hence, the quantum defect of Yb^{3+}-doped laser is typically almost three times lower than that associated with the Nd^{3+}-doped lasers. However, the performance of such a system is intrinsically

* Corresponding author.
E-mail address: ckjaya@yahoo.com (C.K. Jayasankar).

http://dx.doi.org/10.1016/j.jqsrt.2014.02.003
0022-4073

sensitive to temperature since the thermal population of the lower laser level causes absorption at the laser wavelength [2]. Moreover, the Yb^{3+}-doped glasses have been used for the development of solid-state cryocooler for space-borne remote-sensing applications due to the thermally coupled levels at the excited state [3].

Among the various host materials that have been investigated for Yb^{3+} ion doping, so far, phosphate glasses have proven to be potential laser materials as they exhibit high transparency in the visible region, good chemical durability, wider bandwidth, higher efficiencies and low up-conversion characteristics [4]. Moreover, the phosphate glasses exhibit a high gain density due to their high solubility of lanthanide (Ln^{3+}) ions, which allows higher concentrations of active ions to be introduced into a relatively small volume to set a higher gain.

Heavy metal oxides such as PbO play a role as glass modifier in forming the P_2O_5-based glass system which has potential applications as shielding against high-energy radiation including nuclear field [5]. The P_2O_5 is a glass-forming oxide, PbO is a conditional glass former and a combination of these two oxides in the glass matrix result in a low rate of crystallization, moisture resistance, stable and transparent glasses could be achieved due to a dual role played by PbO as a glass former (with PbO_4 structural units, if Pb–O is covalent) as well as the modifier (with PbO_6 structural units, if Pb–O is ionic).

The present work reports the effect of Yb^{3+} ion concentration on the spectroscopic and laser performance parameters in lead-phosphate glasses. Evaluation of oscillator strength by using the Smakula model has been presented. The effect of concentration, glass thickness, optical path length and temperature of the sample on radiation trapping has also been described in detail. The lifetime of the $^2F_{5/2}$ level of Yb^{3+} ion has been investigated at room temperature (RT) and also at low temperatures. The absorption and emission cross-sections have been evaluated from the measured absorption spectra by using the McCumber theory in order to assess their capabilities of being used as a laser active medium.

2. Experimental details

Ytterbium-doped lead-phosphate glasses (PbPhYb) of the composition $40P_2O_5+(26-x)PbO+16K_2O+18Al_2O_3+xYb_2O_3$, where $x=0.1$, 0.5, 1.0, 2.0, 4.0 and 6.0 mol%, were prepared by the melt-quenching technique using high-purity chemicals of $Al(PO_3)_3$, KPO_3, PbO and Yb_2O_3. About 20 g of the batch composition was thoroughly crushed in an agate mortar. The homogeneous mixture was taken in a platinum crucible and heated in an electric furnace at 1075–1125 °C for 1 h. Then the melt was poured onto a brass mold that was preheated and subsequently annealed at 350 °C for 10 h to remove thermal stress and strains. Finally, the glass samples were allowed to RT and polished for their optical measurements.

Refractive index measurements were performed using an Abbe refractometer (ATAGO DR M4) at $\lambda_D=587.6$ nm, $\lambda_F=486.1$ nm and $\lambda_E=656.3$ nm. Fourier transform infrared (FTIR) spectrum of undoped glass was measured using a Perkin Elmer Peragon-500 system. Optical absorption spectra were recorded using a Perkin Elmer Lambda-950 spectrophotometer in the range of 870–1040 nm with a spectral resolution of 0.1 nm. Emission spectra were obtained by exciting with a continuum Titanium sapphire laser and detected with ANDOR spectrum analyzer at RT. Excitation spectra were carried out with a 250 W incandescent lamp passed through a 0.30 m monochromator. For emission decay curves, the samples were excited using an Optical Parametric Oscillator (OPO) with pulses of 10 ns and the signal was registered and averaged using a digital oscilloscope. The low-temperature experiments were performed with a closed cycle helium gas cryogenerator.

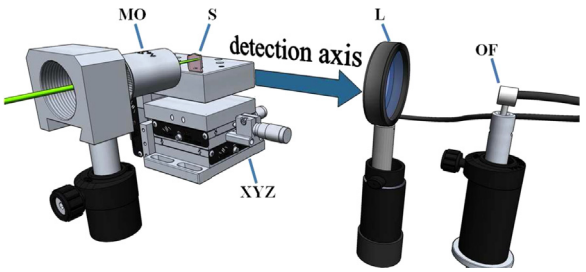

Fig. 1. Experimental set-up employed for the determination of the re-absorption inside the sample. MO – Microscope Objective, S – Sample, XYZ – translation stage, L-Lens and OF-Optical Fiber.

The Yb^{3+} emission trapping or re-absorption was examined by monitoring the spectral shape with increasing the optical path length through the glass. As shown in Fig. 1, the set-up was configured so as to have a 90-degree angle between the excitation and detection axes with the sample placed on a translation stage that allowed it to be moved along the axis of the detection branch. The blue arrow indicates the direction and orientation of the sample translation. The sample was oriented with the narrower side facing the detector and the wider side facing the excitation. A 20× microscope objective lens (Mitutoyo, M-Plan NIR, NA=0.4) was employed to focus the 914 nm excitation beam at points located on the wider face of the sample as the translation stage was moved. The detection branch consisted of a 60 mm convergent lens that focused the emission at the tip of an optical fiber (Thorlabs M25L02, spectral range: 400–2400 nm, core diameter 200 μm, NA 0.22) coupled to ANDOR CCD spectrophotometer with a 0.3 nm spectral resolution. To compare the spectra measured by two different sets of detector equipment, both data were corrected for instrument response.

3. Results and discussion

3.1. Optical properties

Some of the physical and optical properties of Yb^{3+} ions for different concentrations are presented in Table 1. The refractive index of the glass mainly depends on the individual polarizability of cations as well as the cations per unit volume, which increases with increase in the size of the cation. As all the cations are fixed, the refractive index is determined only by the concentration of Yb^{3+} ions per unit volume (molar volume). Refractive index of

Table 1
The glass label, composition and their physical properties (density (d, g/cm^3), thickness (l, mm) concentration (C, $\times 10^{20}$ ions cm^{-3}) refractive index at sodium wavelength (n_D) and oscillator strength (f, $\times 10^{-6}$) for $^2F_{7/2} \rightarrow {}^2F_{5/2}$ transition) of Yb^{3+}:PbPhYb glasses.

Label	Glass composition	d	l	C	n_D	f
PbPhYb01	$40P_2O_5+25.9PbO+16K_2O+18Al_2O_3+0.1\ Yb_2O_3$	3.7	1.68	0.32	1.598	2.32
PbPhYb05	$40P_2O_5+25.5PbO+16K_2O+18Al_2O_3+0.5\ Yb_2O_3$	3.86	1.53	1.56	1.623	2.03
PbPhYb10	$40P_2O_5+24.0PbO+16K_2O+18Al_2O_3+1.0\ Yb_2O_3$	3.9	1.23	3	1.629	1.93
PbPhYb20	$40P_2O_5+23.0PbO+16K_2O+18Al_2O_3+2.0\ Yb_2O_3$	3.96	1.3	6.65	1.635	1.82
PbPhYb40	$40P_2O_5+21.0PbO+16K_2O+18Al_2O_3+4.0\ Yb_2O_3$	4.03	1.7	12.2	1.648	1.79
PbPhYb60	$40P_2O_5+19.0PbO+16K_2O+18Al_2O_3+6.0\ Yb_2O_3$	4.21	1.52	18.43	1.657	1.71

Yb_2O_3-doped glasses at different wavelengths is shown in Fig. 2(a). As can be seen from Fig. 2(a), the refractive index increases linearly with increase in Yb_2O_3 concentration, which may be due to the increase of higher atomic weight, but it decreases with increase of the spectral line wavelength. The refractive indices of 1.0 mol% Yb_2O_3-doped glass were found to be $n_F=1.6293$, $n_D=1.6199$ and $n_E=1.6156$. The linear increase of refractive index is mainly ascribed to the concentration of Yb_2O_3 with high average electronic polarizability [6].

Nonlinear refractive index (n_2) and nonlinear refractive index coefficient (γ) are important parameters for a laser glass. Direct measurement of γ is difficult, so the empirical relation developed by Boling et al. [7] for γ from the refractive index (n_D) and the Abbe number (ν_d) of the glass can be used. The n_2 is given by $n_2=cn_D\gamma/40\pi$ where

$$\gamma = \frac{K(n_D-1)(n_D^2+2)^2}{n_D\nu_d[1.52+(n_D^2+2)(n_D+1)\nu_d/6n_D]^{1/2}} \quad (1)$$

where K is the empirically determined constant, which equals 2.8×10^{-18} m^2/W, c is the velocity of light and ν_d is the Abbe number defined as $\nu_d=(n_D-1)/(n_F-n_E)$. The glass with high refractive index is supposed to have relatively low Abbe number, which leads to higher dispersion. The variation of ν_d and n_2 as a function of Yb_2O_3 concentration is shown in Fig. 2(b). From Fig. 2(b), the Abbe number decreases whereas n_2 increases slightly up to 4.0 mol% concentration and then reverses in its trend. This trend indicating that the dispersion is low may be due to the dependence of partial dispersion (n_F-n_C) and n_D on the wavelength being almost constant, i.e., not significantly varying with Yb_2O_3 concentration. The n_2 and γ values are found to be 1.63×10^{-13} esu and 4.21×10^{-20} m^2/W, respectively, for PbPhYb glass. For most of the commercial laser glasses, the magnitudes of n_2 ($\times10^{-13}$ esu) and γ ($\times10^{-20}$ m^2/W) are found to be in the ranges of 1.01–1.04 and 2.78–3.6 [4]. The higher values of n_2 and γ for the lead phosphate glasses may be due to the presence of heavy metal oxide such as PbO content. Moreover, Abbe number for the PbPhYb glasses slightly decreases to 25.1 but it could be constant around 25.1–26.8.

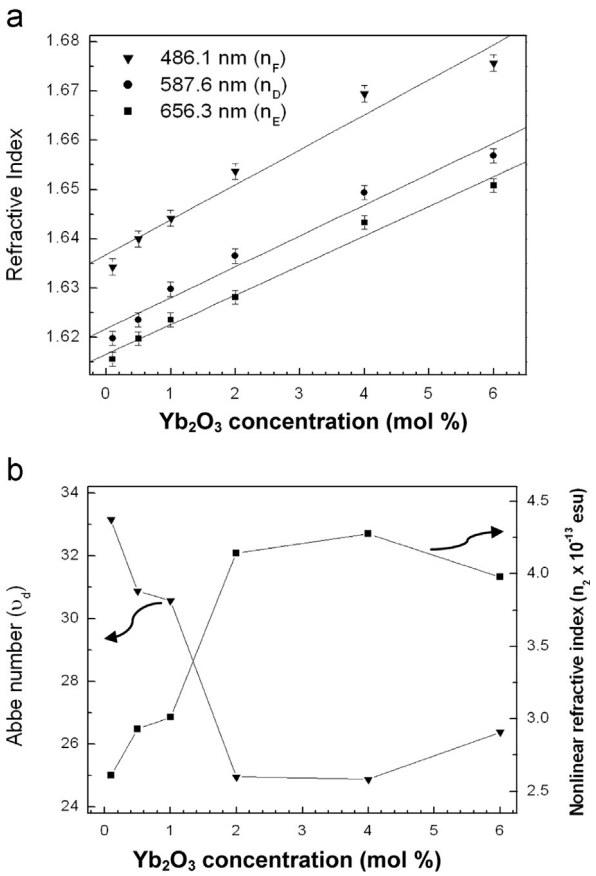

Fig. 2. (a) Refractive index at different wavelengths. (b) Variation of Abbe number and non-linear refractive index for Yb^{3+}:PbPhYb glasses (lines are used as guide to the eyes).

3.2. Structural properties

Fig. 3(a) shows the FTIR spectrum of undoped lead phosphate glass. The observed transmission bands from 1000 to 1110 cm^{-1} are due to PO_3^{2-} and PO_4^{2-} symmetrical stretching vibration, which may be due to the symmetric stretching of PO_2 terminal groups. The vibrational modes at 895–900 cm^{-1} are due to P–O–P asymmetrical stretch groups, which are also dominant. The transmission bands at 765–770 cm^{-1} and 478–485 cm^{-1} correspond to the symmetric vibration of the P–O–P bond and the P–O–(PO_4^{3-}) deformation modes, respectively. The band at 2850–2920 cm^{-1} corresponds to P–OH linkages of the host. The relatively wide and strong bands at around 3450 cm^{-1} are due to asymmetric stretching vibrations of free OH^- groups which are also observed in other reported phosphate glasses [8].

Fig. 3(b) shows the Raman spectrum for the undoped lead phosphate glass exhibiting seven bands at 336, 470,

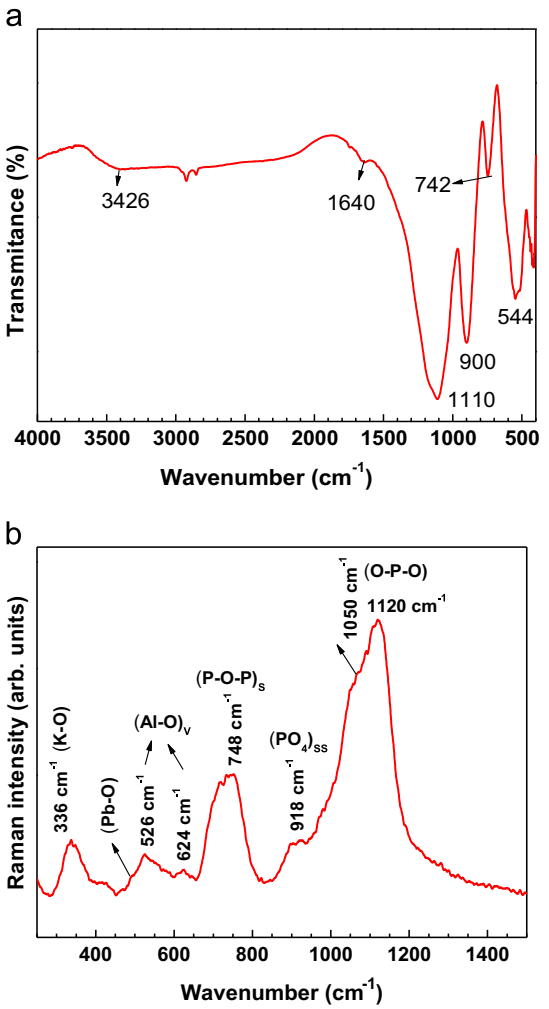

Fig. 3. (a) FTIR and (b) Raman spectrum of undoped lead-phosphate glass.

526, 624, 748, 918, 1050 and 1120 cm^{-1}. The observed bands are related to characteristic phosphate group vibrations. The band at 1120 cm^{-1} is ascribable to the vibration of O–P–O nonbridging oxygen (NBO) $(PO_2)_S$ indicating the formation of Q^2 phosphate tetrahedra. The band at 918 cm^{-1} might be due to the (PO_4) symmetric stretching vibrations (SSV) of the Q^0 (Q^0 represents the no bridging oxygen per tetrahedron) species [9]. The increase of Q^0 groups is due to the breaking of phosphate chains [10]. The broad band at 748 cm^{-1} is assigned to the vibrations of $(P–O–P)_s$ stretch in very short phosphate chains or in ring structure [11]. The bands at 526 and 624 cm^{-1} belong to Al_2O_3 vibrations [12]. The peak at 470 cm^{-1} is related to symmetric bending vibration of Pb–O in PbO_4 tetragonal pyramid (PbO covalent bond), which is due to the glass-forming ability of PbO. Relatively strong band at around 336 cm^{-1} is due to alkali-oxides (such as K_2O and Na_2O) [13]. It is known that the phonon energy of the host can be defined as the highest vibrational energy of the host which is found to be 1120 cm^{-1} and plays a major role in the optical properties of the luminescent ions.

3.3. Spectroscopic properties

The performance of Yb^{3+}-glass laser can be accessed from effective absorption and emission cross-sections of $4f^{13}$–$4f^{13}$ transitions and lifetimes of the $^2F_{5/2}$ fluorescent level. These parameters can be obtained from absorption and emission spectra. The absorption cross-section for the $^2F_{7/2}\rightarrow{}^2F_{5/2}$ transition of Yb^{3+} ion can be obtained by using the following equation [14,15]:

$$\sigma_{ab}=\frac{2.303OD}{C.l} \tag{2}$$

where OD is the optical density, C is the Yb^{3+} ion concentration and l is the thickness of the glass sample.

The emission cross-section $\sigma_{em}(\lambda)$ can be evaluated from the reciprocity method described by McCumber (McC) [16] using the measured absorption cross-section (σ_{ab}):

$$\sigma_{em}(\lambda)=\sigma_{ab}(\lambda)\frac{Z_l}{Z_u}\exp\left(\frac{E_{ZL}-hc\lambda^{-1}}{kT}\right) \tag{3}$$

where Z_l and Z_u are the partial functions of the lower (ground) and upper (excited) levels, respectively; and E_{ZL} is the zero-line energy which is equal to the energy separation between the lowest Stark components of the upper and lower levels of the Yb^{3+} ion. The h and k are the Planck and the Boltzmann constants, respectively. The ratio of the partial functions Z_l/Z_u becomes the degeneracy weighing of the two states corresponding to the $^2F_{7/2}\rightarrow{}^2F_{5/2}$ absorption transitions, and since this ratio does not change significantly with the change of chemical compositions, it is equal to 4/3 at RT.

The emission cross-section $\sigma_{em}(\lambda)$ can also be obtained from the Füchtbauer–Landenburg (F–L) equation [17] and for the $^2F_{5/2}\rightarrow{}^2F_{7/2}$ transition of Yb^{3+} ions it is expressed as

$$\sigma_{em}(\lambda)=\frac{\lambda_p^4Ag(\lambda)}{8\pi cn^2\Delta\lambda_{eff}} \tag{4}$$

where A is the spontaneous transition probability of the $^2F_{5/2}\rightarrow{}^2F_{7/2}$ transition and is determined from the absorption spectra by using the following relationship:

$$A=\frac{1}{\tau_R}=\frac{8\pi cn^2(2J^1+1)}{\lambda_p^4(2J+1)}\int\alpha(\lambda)d\lambda \tag{5}$$

where J^1 and J are the total angular momentum for the upper and lower levels, respectively; λ_p is the absorption peak wavelength; n is the refractive index; and $g(\lambda)$ is the normalized line shape function of the measured emission transition of the Yb^{3+} ion. The F–L equation has been used to determine the emission cross-sections to confirm the quality of the calculated results obtained by the McC method [16].

Another interesting spectroscopic parameter for the optical characterization of the Yb^{3+} luminescence is the effective line width ($\Delta\lambda_{eff}$), which is expressed as

$$\Delta\lambda_{eff}=\int\frac{I(\lambda)d\lambda}{I_{\max}} \tag{6}$$

where $I(\lambda)$ is the intensity at the wavelength λ; and I_{max} is the intensity at the peak wavelength λ_p.

The oscillator strength for the $^2F_{7/2} \rightarrow {}^2F_{5/2}$ transition of Yb^{3+} ion was estimated using the Smakula model [18] as there is only one excited level for the Yb^{3+} ion. Therefore, it is not feasible to evaluate the oscillator strength for this transition using the Judd–Ofelt (JO) theory. The Smakula model states that the correlation between the integrated absorption coefficient ($\int \alpha(E)dE$) and oscillator strength (f_{ed}) depends not only on the index of refraction (n) but also on the number density of the ions (N/V). If the Yb^{3+} transition is due to the electric-dipole contribution, the expression for the oscillator strength between the ground and exited states can be evaluated from the Smakula equation as follows:

$$f_{ed} = 0.821 \times 10^{17} \frac{n}{(n^2+2)^2} \left(\frac{V}{N}\right) \int_{band} \alpha(\lambda) d\lambda \quad (7)$$

where n is the refractive index of glass, N/V is the number density of the Yb^{3+} ion in ions/cm^3, and $\int_{band}\alpha(\lambda)d\lambda$ is the integrated absorption coefficient (area under absorption cross-section curve) of the band.

Since $^2F_{7/2} \rightarrow {}^2F_{5/2}$ transition is partly allowed, the magnetic-dipole contribution plays a vital role while calculating the total oscillator strength of the transition. The magnitude of magnetic-dipole oscillator strength (f_{md}) [$(17.76 \times 10^{-8}) \times$ index of refraction (n)] was taken from the work of Carnall et al. [19] to estimate the total oscillator strength ($f = f_{ed} + f_{md}$) of the transition and the values are presented in Table 1. As can be seen from Table 1, the decrease in oscillator strength with increase in Yb^{3+} ion concentration is due to the direct dependence of oscillator strength (f_{ed}) on Integrated absorption coefficient [$(V/N)\int \alpha(E)dE$], which decreases with increase in Yb^{3+} ion concentration. The integrated absorption increase linearly with increase in Yb^{3+} ion number density (N/V), which is inversely proportional to the oscillator strength (see Eq. (6)). However, increase in oscillator strength could be due to the increase in refractive index of the glass with increase in Yb_2O_3 concentration. These values are in good concurrence with the data evaluated by the same model for the other Yb^{3+}-doped barium–thorium fluoride [20] and tellurite [21] glasses. The dipole transition in an isolated ion at lower concentration is always stronger than that of the higher concentrations where the energy migration/transfer among dopant ions increases due to reduction in Yb–Yb interionic distance reduction [22,23].

Fig. 4 shows the concentration-dependent absorption spectra of Yb^{3+} ions in PbPhYb glasses. The profile of the absorption spectra is similar for all the samples, except for variation in their intensities. The inhomogeneously broadened spectra correspond to the transition between the Stark sublevels of ground ($^2F_{7/2}$) and excited ($^2F_{5/2}$) levels. The broad absorption bands due to the electronic transition of the Stark sublevels as well as strong electron–phonon interaction represent the glassy host. The absorption spectrum was deconvoluted into five Gaussian peaks centered at around 915 nm (10,928 cm^{-1}), 925 nm (10,811 cm^{-1}), 960 nm (10,438 cm^{-1}), 975 nm (10,256 cm^{-1}) and 998 nm (10,020 cm^{-1}) are labeled as $a \rightarrow c^1$, $b \rightarrow c^1$, $a \rightarrow b^1$, $a \rightarrow a^1$ and $c \rightarrow a^1$, respectively, which correspond to different transitions between Stark levels of $^2F_{5/2}$ and $^2F_{7/2}$ (Fig. 4(a)) with the help of the energy-level diagram (Fig. 4(b)). Almost a linear variation of optical density (0.023–0.62) absorption coefficient (α) is observed with increase in Yb_2O_3 concentration (inset of Fig. 4(a)), which indicates that the presence of similar local environment around the Yb^{3+} ions in PbPhYb glasses.

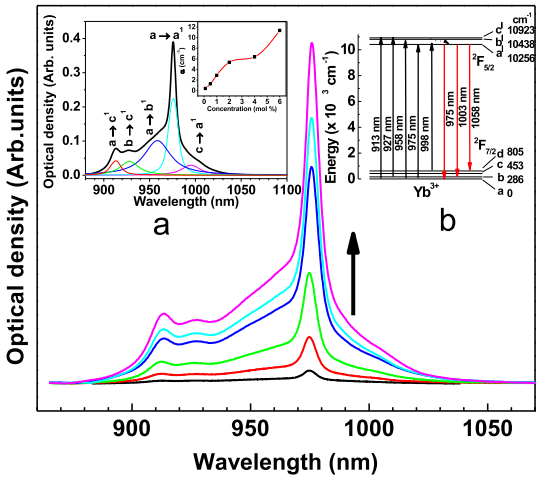

Fig. 4. Concentration-dependent absorption spectra of Yb^{3+}:PbPhYb glasses. (a) Deconvoluted absorption spectrum and the inset shows the variation of absorption coefficient with concentration. (b) Energy-level diagram of Yb^{3+} ion representing absorption and emission channels.

Fig. 5(a) shows the NIR emission spectra of Yb^{3+}-doped lead phosphate glasses for different Yb_2O_3 concentrations. The emission spectra normalized to primary peak (at 975 nm), the secondary peak (at 1003 nm) increases along with peak positions, which shift towards longer wavelengths (red shift) with increase in Yb_2O_3 concentration. Fig. 5(b) shows the integrated intensities, by deconvolution with the Gaussian fit of primary and secondary peaks increase with increase in Yb^{3+} ion concentration. This behavior may be due to the radiation trapping or re-absorption as well as energy migration [24] among the Yb^{3+} ions. The amount of radiation trapping was estimated by radiation trapping coefficient (rtc) [25,26], which increases with increase in Yb_2O_3 concentration due to the increase of trapping at higher concentrations (see Table 2) and a similar behavior was also observed in those of other reported Yb^{3+}-doped phosphate [25] and heavy metal oxide [27] glasses. The observation of the two-step dependence may be due to the increased radiation trapping effect at higher concentrations, which is also evidenced from the radiation trapping coefficient (see Table 2). The emission spectrum shows three peaks, centered at 975 nm (10,256 cm^{-1}), 1003 nm (9970 cm^{-1}) and 1058 nm (9451 cm^{-1}), and are labeled as $a^1 \rightarrow a$, $a^1 \rightarrow b$ and $a^1 \rightarrow d$, respectively, as shown in the inset of Fig. 5(b). Although the emission intensity is proportional to the Yb^{3+} ion concentration, the profile of the emission spectra exhibits notable changes, which may be due to the effect of radiation trapping. This effect depends on Yb^{3+} ion concentration [25,27–29] and thickness of the glasses [21,30].

In addition to the above two possibilities on the effect of radiation trapping, the present study focuses on the interaction of Yb^{3+} ions along the optical path and also at

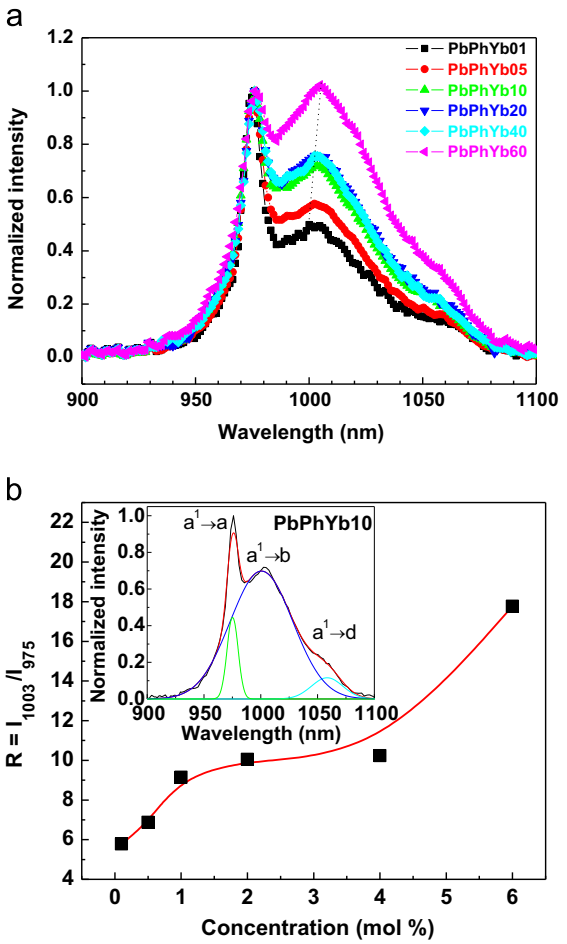

Fig. 5. (a) Emission spectra of Yb^{3+}:PbPhYb glasses for different concentrations. (b)Variation of integrated intensity ratio of primary (I_{975}) and secondary (I_{1003}) peaks for different concentrations and the inset shows the deconvoluted emission spectrum (lines are used as guide to the eyes).

Table 2
Comparison between the Füchtbauer–Landenburg (F–L) and McCumber (McC) methods of emission cross-sections at primary (λ_p) and secondary (λ_0) wavelengths, their ratios and radiative trapping coefficient (rtc) for Yb^{3+}:PbPhYb glasses.

Glasses	$\sigma_{emp}(\lambda_p)$ ($\times 10^{-20}$ cm^2)		$\sigma_{ems}(\lambda_0)$ ($\times 10^{-20}$ cm^2)		$\sigma_{ems}/\sigma_{emp}$		rtc
	FL	McC	FL	McC	FL	McC	
PbPhYb01	0.92	1.81	0.52	0.99	0.56	0.55	0.18
PbPhYb05	0.61	11.84	0.51	5.68	0.83	0.48	0.72
PbPhYb10	0.71	1.35	0.51	0.63	0.71	0.46	0.53
PbPhYb20	0.6	1.12	0.5	0.48	0.83	0.42	0.97
PbPhYb40	0.39	1.32	0.49	0.46	0.83	0.35	1.37
PbPhYb60	0.46	0.88	0.48	0.31	1.04	0.35	1.97

low temperatures. In the first case (effect of concentration) radiation trapping is evaluated by taking the integrated intensities of the deconvoluted bands centered at 975 nm (area I_{975}) and 1003 nm (area I_{1003}), as represented in Fig. 5(b) (without considering the weak band at 1058 nm), the integrated intensity ratio at different concentrations

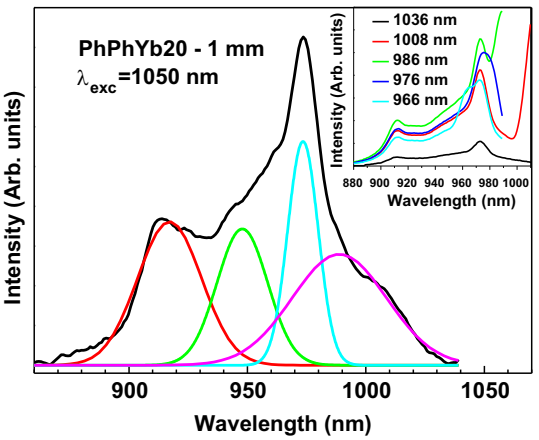

Fig. 6. The excitation spectrum of 2.0 mol% Yb_2O_3-doped glass (1 mm thickness) and the inset shows the excitation spectra by monitoring at different wavelengths.

exhibits the variant changes due to radiation trapping. Moreover, the profile of the emission spectra broadens, which results in an increase in the effective bandwidth ($\Delta\lambda_{eff}$) with increase in Yb_2O_3 concentration.

Fig. 6 shows the excitation spectrum of 2.0 mol% Yb^{3+}-doped glass (1 mm thickness) by monitoring at 1050 nm emission. The spectrum shows four bands by deconvolution with the Gaussian fit, which are due to transitions from ground state to the various Stark levels of the excited state, which also is in good concurrence with the absorption spectrum. The excitation spectra by monitoring the emission at 966, 976, 986, 1008 and 1036 nm are shown in the inset of Fig. 6. The spectra show similar profile except for their intensity and peak positions at the primary peak.

In the second case (effect of sample thickness), emitted light inside the sample takes many absorption–emission paths. It is well known that the radiation trapping effect can be realized as a function of sample thickness [30]. Fig. 7(a) shows the emission spectra of 2.0 mol% Yb_2O_3-doped glass as a function of sample thickness measured at the edge of the sample. As can be seen from Fig. 7(a), the spectra normalized to the primary peak and variation can be seen at the secondary peak. With increase in sample thickness, one can clearly observe the spectral intensity at the secondary peak increases and also broadens with the interaction of more numbers of Yb^{3+} ions; as a consequence, the peak wavelength is red shifted. The above observations clearly demonstrate that radiation trapping is predominant in the present glasses.

In the third case (optical path length), radiation trapping is also investigated by the detection of emitted photons through the optical path and the set-up used for this study is shown in Fig. 1. The emission spectra were recorded at different positions of 2.0 mol% Yb_2O_3-doped glass (1 mm thickness), shown in Fig. 7(b). To compare the relative intensities of the secondary peak, all the spectra were normalized to the intensity of the primary peak. As observed from Fig. 7(b), the emission intensity increases and also broadens (2 nm) when the interaction of the laser moves from the edge towards the center of the sample due to re-absorption. These results are in good concurrence with

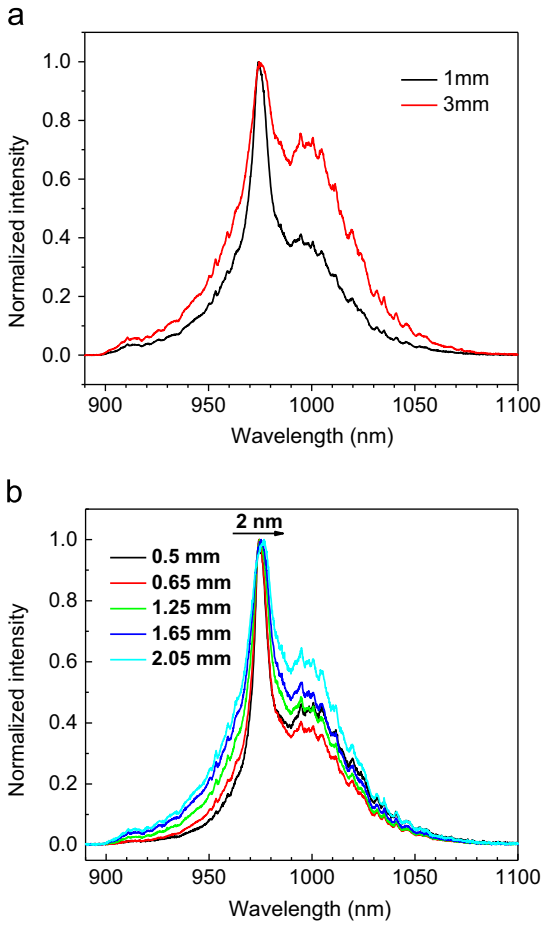

Fig. 7. Emission spectra at 1 and 3 mm thicknesses (a) and different positions (b) of the sample.

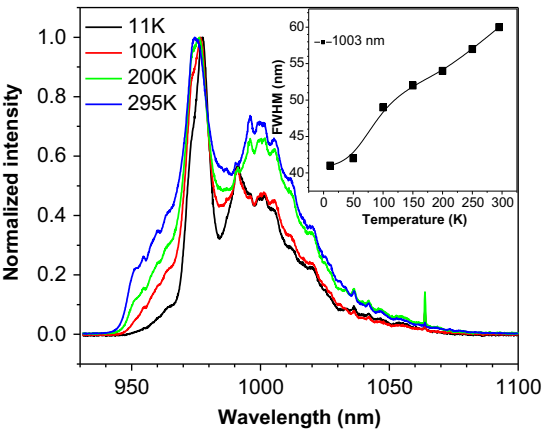

Fig. 8. Emission spectra for 2.0 mol% Yb_2O_3-doped glass (3 mm thickness) at different temperatures and the inset shows the variation FWHM of 1003 nm peak at different temperatures. (Lines are used as guide to the eyes).

the fact that the radiation trapping effects on the spectra are more pronounced with increase in concentration.

Laser-induced cooling of solids by anti-Stokes fluorescence of blue shifted photons with high energy was proved experimentally in Yb^{3+} – doped ZBLAN glass by Epstein et al. [31]. Thereafter much work has been devoted on the cooling of solids in various Yb^{3+}-doped solid materials [3]. Fig. 8 shows the emission spectra of PbPhYb20 (3 mm thickness) glass as a function of temperature. As seen from Fig. 8, the short wavelength of the blue tail and also at secondary peaks of the emission spectra decreases at low temperatures. The spectra show emission at 990 and 1003 nm, which have energies at 155 and 337 cm^{-1}, respectively, above the $a^1 \rightarrow a$ transition (see Fig. 4(b)). At higher temperatures it shows a smooth band raise which is due to the broadening of the states particularly at level 'a^1'. In addition to the emission intensity and peak position (3 nm) broadening of the profile also decreases when the temperature dips to cryogenic temperature (11 K). As the temperature increases, the peak position at 975 nm decreases due to broadening around the shoulders where as the variation of FWHM with temperature is shown in the inset of Fig. 8, which increases from 41 nm at cryogenic temperature (11 K) to 60 nm at RT. The increase in FWHM is due to the homogeneous broadening caused by non-radiative relaxation.

The decay rate of the $^2F_{5/2}$ level is represented by [15]

$$\frac{1}{\tau_f} = \frac{1}{\tau_{rad}} + W_{MPR} + W_{ET} \tag{8}$$

where τ_f and τ_{rad} are the experimental lifetime and radiative lifetimes, respectively. W_{MPR} is the multi-phonon relaxation (MPR) rate, which can be neglected due to the large energy gap between $^2F_{5/2}$ and $^2F_{7/2}$ levels; W_{ET} includes the energy migration and other transfer processes (the energy transfer rate between Yb^{3+} and OH^- radicals).

The measurement of lifetime is quite difficult because of the mixing of the two processes at the excited state: radiation trapping and self-quenching. In the earlier one the emitted radiation may be reabsorbed (radiative transfer) and the later one is produced by the migration towards (non-radiative transfer) uncontrolled traps and intrinsic quenching centers. [32–34]. The longer lifetime permits higher population inversion, which is an important feature for laser operation.

The luminescence decay curves at RT for the $^2F_{5/2} \rightarrow {}^2F_{7/2}$ transition of Yb^{3+} ions are found to be single exponential for all the concentrations and are shown in Fig. 9(a). The fluorescence lifetime (τ_f) of Yb^{3+} ion from the $^2F_{5/2}$ level shortens (see inset of Fig. 9(a)) after an initial increase (1.05–1.17 ms), from 1.17 to 0.54 ms, which indicates quenching of lifetime, whereas the radiative lifetime determined from the radiative transition probability (A_{rad}), which increases from 1.25 to 4.13 ms with increase in Yb_2O_3 concentration. The decrease in lifetime could be due to the concentration quenching (self-quenching) at higher concentrations and increase in lifetime due to radiation trapping at the lower concentrations. Therefore, the quenching of lifetime may also be either due to interactions: (i) between Yb^{3+} and OH^- radicals being dominant at lower Yb^{3+} ions concentration ($N_{Yb} \sim 3 \times 10^{20}$ ions/cc); and (ii) the Yb^{3+}-other impurities being dominant at higher Yb^{3+} ion concentration. The magnitudes of τ_f for

Yb^{3+}-doped systems are compared with the other reported glasses [23,25,35–42] and presented in Table 4. It is also observed that the τ_f of PbPhYb05 glass is higher than those of the other reported silica [23], $20Bi(PO_3)_3$–$10Sr(PO_3)_3$–$35BaF_2$–$35MgF_2$ (BSBM) [35], $0.4MgF_2$–$0.4BaF_2$–$0.1Al(PO_3)_3$–$0.1Ba(PO_3)_2$ (MBABP) [36], $58.95P_2O_5$–$17K_2O$–$14.95BaO$–$9Al_2O_3$–$0.1Yb_2O_3$ (PKBAYb01) [40] and $53.95P_2O_5$–$14K_2O$–$10KF$–$12.95BaO$–$9Al_2O_3$–$0.1Yb_2O_3$ (PKFBAYb01) [41] glasses and lower than $LiYb_xLa_{(1-x)}P_4O_{12}$ (PLY) [25], $60SiO_2$–$20Al_2O_3$–$20CaF_2$ (SACF0.2) [37], FP [38], $25P_2O_5$–$20Nb_2O_5$–$24CaO$–$10SrO$–$20BaO$ (PN-20) [39], $18P_2O_5$–$18Nb_2O_5$–$13B_2O_3$–$20ZnO$–$15SrO$–$15BaO$ (PNB-18) [39], $(60–65)P_2O_5$–$(4–8)B_2O_3$–$(5–10)Al_2O_3$–$(5–10)BaO$–$(0–2)La_2O_3$–$(0–2)Nb_2O_3$ (New/Yb) [40] and Kigre QX/Yb [40] glasses. As seen from Table 4, the decrease in quantum efficiency (η) with increase in Yb_2O_3 concentration may be due to the reduction of Yb^{3+} intrinsic distances which leads to migration of energy among the Yb^{3+} ions [43] followed by coupling with OH^- radicals found to be more probable in PbPhYb glasses.

Fig. 9(b) shows the decay curves of the excited $^2F_{5/2}$ level of Yb^{3+} ion were measured at different temperatures

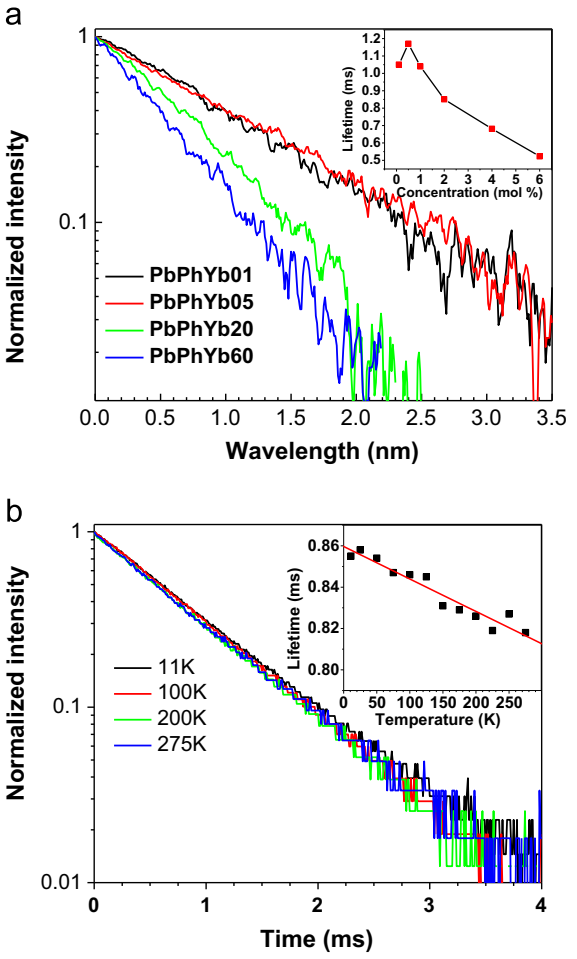

Fig. 9. (a) Decay curves of $^2F_{5/2}$ level for different Yb^{3+} ion concentrations and the inset shows the variation of lifetime with temperature. (b) Decay curves for 2.0 mol% doped glass and the inset shows the variation of lifetime at different temperatures (for the sake of clarity selected decay curves only presented). (Lines are used as guide to the eyes).

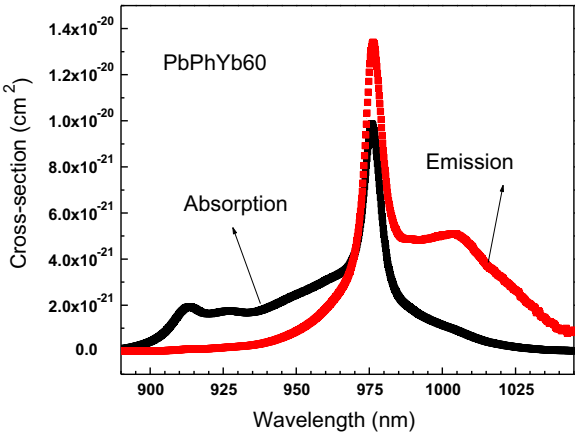

Fig. 10. Absorption and emission cross-section spectra of 6.0 mol% Yb_2O_3-doped PbPhYb60 glass.

for the 2.0 mol% doped glass (3 mm thickness). For the sake of clarity, only some of the selected temperatures are presented. The decay curves exhibit single exponential nature and the lifetimes were determined by using a single exponential decay function. It is found that the lifetime increases (0.82–0.86 ms) with decrease in temperature (275–11 K) due to depopulation and also increases the radiation trapping at the excited manifold, shown in the inset of Fig. 9(b). This effect probably is due to a reduction in the quenching processes among the Yb^{3+} ions. The higher lifetime was found at low temperatures due to radiation trapping whereas the lower lifetimes at higher temperatures are due to self-quenching. The lifetime increases nearly 6% as the temperature reduces to cryogenic temperature (11 K) when compared with the RT.

The absorption cross-section of Yb^{3+} ions was evaluated for the $^2F_{7/2} \rightarrow {}^2F_{5/2}$ transition by using the measured absorption spectra. Initially, the absorption cross-section increases and then decreases with increase in Yb_2O_3 concentration due to the formation of clusters [44]. These assumptions are further evidenced by the decrease in emission cross-sections ($\sigma_{em}(\lambda)$) at primary (975 nm) and secondary (1.0 μm) peaks with increase in Yb_2O_3 concentration. The $\sigma_{em}(\lambda)$ can be evaluated from the reciprocity method described by the McCumber (McC) [16] theory using the measured absorption cross-section (σ_{ab}) to avoid the radiation trapping effect. Fig. 10 shows the absorption and emission cross-section spectra of 6.0 mol% Yb_2O_3-doped glass. The emission cross-section can also be obtained from Füchtbauer–Landenburg (F–L) formula [17] that requires the radiative transition probability and emission line shape for the $^2F_{5/2} \rightarrow {}^2F_{7/2}$ transition of Yb^{3+} ions, which includes the radiation trapping. Both the absorption and emission cross-sections have shown a strong dependence on Yb_2O_3 concentration. Some of the spectroscopic and laser performance parameters are presented in Table 3. It is observed from Table 3 that the value of σ_{ab} (10^{-20} cm^2) is found to vary from 8.51 to 0.63 whereas the $\sigma_{em}(\lambda_p)$ (10^{-20} cm^2) varies from 11.84 to 0.8 and $\sigma_{em}(\lambda_0)$ varies from 5.68 to 0.31 with increase in Yb_2O_3 concentration. Higher absorption and emission cross-sections were obtained for PbPhYb05 glass and found to be higher than

Table 3
Spectroscopic and laser performance properties of Yb^{3+}-doped PbPhYb glasses.

Glasses	$\sigma_{ab}(\lambda_p)$ ($\times 10^{-20}$ cm^2)	$\sigma_{ab}(\lambda_0)$ ($\times 10^{-20}$ cm^2)	λ_p (nm)	λ_0 (nm)	$\Delta\lambda_{eff}$ (nm)	A (s^{-1})	W_{nr}	τ_f (ms)	η (%)	β_{min}	I_{sat} (kW/cm^2)	I_{min} (kW/cm^2)	$\sigma_{ab}(\lambda_p)\times\tau_f$ (cm^2.ms)	$\sigma_{em}(\lambda_0)\times\tau_f$ (cm^2.ms)	τ_{min} (fs)	G (cm^2 ms)	U_{sat} (J/cm^2)
PbPhYb01	1.31	0.22	975.6	1005	39	795	0.15	1.05	83	0.18	14.05	2.69	1.37	1.03	86	42.5	16.85
PbPhYb05	8.51	1.16	975.6	1004	32	436	0.35	1.17	58	0.17	2.02	0.34	9.95	6.64	104	0.88	2.98
PbPhYb10	0.96	0.12	976	1003	32	499	0.52	1.04	45	0.16	20.41	3.26	0.99	0.65	104	1.89	27.18
PbPhYb20	0.95	0.1	975.8	1003	29	395	0.75	0.82	34	0.17	24.23	4.17	0.83	0.41	111	2.65	35.16
PbPhYb40	0.81	0.09	975.8	1002	28	242	1.06	0.74	21	0.18	34.12	6.23	0.59	0.33	119	3.29	37.08
PbPhYb60	0.63	0.06	975.6	1000	27	287	1.61	0.54	13	0.16	59.13	9.61	0.34	0.17	123	1.94	55.13

those of other reported phosphate [25,35,36,39–42] and silicate glasses [23,38].

The Yb^{3+}-doped laser glasses involve the evaluation of laser performance parameters in addition to the above-mentioned spectroscopic properties. The excited Yb^{3+} ions to balance the gain with the ground state absorption at laser wavelength λ_0 are known as β_{min}; pump saturation intensity (I_{sat}) and minimum absorbed pump intensity (I_{min}) were evaluated [17]. The β_{min} and I_{sat} should be as low as possible to achieve highly intense lasers. The β_{min} values are independent whereas I_{sat} and I_{min} increase with increase in Yb_2O_3 concentration. The gain coefficient (G) [45] is closely related to the product of the absorption cross-section, $\sigma_{ab}(\lambda_p)$, emission cross-section, $\sigma_{em}(\lambda_0)$, and luminescence lifetime (τ_f). Therefore, it has been suggested that the laser glass should have a higher gain coefficient, G, for laser applications. The value of G decreases with increase in concentration due to the decrease in absorption and emission cross-section and lifetime. The product of $\sigma_{ab}(\lambda_p)\times\tau_f$ as well as $\sigma_{em}(\lambda_0)\times\tau_f$ decreases with increase in Yb_2O_3 concentration due to energy migration, which leads to continuous decrease in the values of $\sigma_{ab}(\lambda_p)$, $\sigma_{em}(\lambda_0)$ and τ_f.

High intensity lasers produce ultrafast laser pulses with a given amount of optical energy, both temporal and spatial. The temporal limit is expressed by the time bandwidth product, $\tau_{min}=\lambda_0^2/(c\times\Delta\lambda_{eff})$ [46], where τ_{min} is the minimum pulse duration and $\Delta\lambda_{eff}$ is the fluorescence bandwidth. The value of τ_{min} increases with increase in Yb_2O_3 concentration. The storage of optical energy [46] is one of the important properties which depends on spontaneous emission and pump power when the laser materials involve higher doping concentration as well as longer lifetime and are essential to create population inversion in the gain media.

The wavelength dependent gain cross-section (σ_g) leads to an estimation of the probable laser wavelength, which can be obtained as $\sigma_g(\lambda)=\beta\sigma_{em}(\lambda)-(1-\beta)\sigma_{ab}(\lambda)$, where β is the inversion population of Yb^{3+} ions. The wavelength dependence of the gain cross-section was calculated for several values of population inversion β (β=0, 0.1, 0.2,…, 1) and is shown in Fig. 11. It displays that a wide tunable wavelength range from 990 to 1030 nm is expected when β is larger than 0.4. The results at RT and cryogenic temperatures suggest that the studied glasses could be considered for high energy and high power laser applications as well as cryocoolers.

4. Conclusions

Yb^{3+}-doped lead phosphate glasses were synthesized and their optical, spectroscopic and laser parameters characterized. Linear refractive index, Abbe number and non-linear refractive index were investigated systematically as a function of Yb_2O_3 concentration, which are found to be higher than those of the other reported phosphate glasses due to the presence of heavy metal oxide (PbO). The oscillator strength of the absorption transition was determined using the Smakula model due to the unfeasibility of the Judd–Ofelt theory. The profile of the emission spectra changed with concentration, optical

Table 4
Spectroscopic and laser performance parameters of Yb^{3+}-doped systems.

Systems	Parameters						
	λ_0 (nm)	$\sigma_{ab}(\lambda_p)$ ($\times 10^{-20}$ cm^2)	$\sigma_{em}(\lambda_0)$ ($\times 10^{-20}$ cm^2)	τ_f (ms)	I_{min} (kW/cm^2)	$\sigma_{ab}(\lambda_p)$ x τ_f ($\times 10^{-20}$ cm^2 ms)	$\sigma_{em}(\lambda_0)$ x τ_f ($\times 10^{-20}$ cm^2 ms)
PbPhYb05	1004	8.51	5.68	1.17	0.34	9.95	6.64
Silica glass [23]	1032	2.4	0.77	0.78	0.71	1.87	0.6
PLY [25]	1004	0.99	0.72	1.21	1.89	1.19	0.87
BSBM [35]	977	1.77	1.39	0.71	3.7	1.25	0.98
MBABP [36]	976	1.64	0.87	0.65	–	1.06	0.57
SACF0.2 [37]	975	1.19	–	1.29	2.43	1.53	–
FP [38]	1020	0.43	0.5	1.2	0.8	0.52	0.6
PN-20 [39]	1035	1	1.35	1.36	0.6	1.36	1.84
PNB-18 [39]	1016	0.68	1.08	2	1.3	1.36	2.16
New/Yb [40]	975	0.53	–	2.2	–	1.06	–
Kigre QX/Yb [40]	976	1.06	–	2	–	1.12	–
PKBAYb01 [41]	1002	1.71	0.14	1.15	1.89	1.97	0.72
PKFBAYb01 [42]	1008	1.5	0.77	1.15	0.66	1.72	0.8

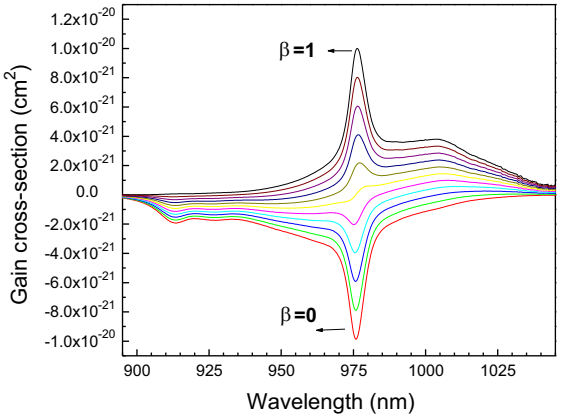

Fig. 11. Gain cross-section of 6.0 mol% Yb^{3+}-doped PbPhYb60 glasses.

path, temperature and thickness of the sample due to radiation trapping. The emission cross-section is evaluated from the absorption cross-section using the McCumber theory, which is found to be higher than those of the other reported glasses. The possibility of achieving laser action was estimated around $I_{min}=0.34$ kW/cm^2. The lifetime is found to decrease with increase in Yb^{3+} ion concentration and temperature, which revealed the self-quenching and energy migration among the Yb^{3+} ions. Spectral properties such as absorption and emission cross-sections and gain cross-section of the lead phosphate glasses are found to be higher than those of commonly occurring phosphate glasses. The results of RT and low temperature reveal that the investigated glasses have potential applications as cryocooled high energy and high power lasers.

Acknowledgment

One of the authors (C.K.J) is grateful to DAE-BRNS (No. 2007/34/25-BRNS/2415), Mumbai, Govt. of India for the award of the major research project.

References

[1] Rutherford TS, Tulloch WM, Sinha S, Byer RL. Yb:YAG and Nd:YAG edge-pumped slab lasers. Opt Lett 2001;26:986–9.
[2] Diening A, Mobert PEA, Huber G. Diode-pumped continuous-wave, quasi-continuous-wave, and Q-switched laser operation of Yb^{3+}, Tm^{3+}: YLiF4 at 1.5 and 2.3 μm. J Appl Phys 1998;84:5900–4.
[3] Murtagh MT, Sigel Jr GH, Fajardo JC, Edwards BC, Epstein RI. Composition investigation of Yb^{3+}-doped heavy metal oxide fluoride glasses for laser-induced fluorescent cooling applications. J Non-Cryst Solids 1999;256 & 257:207–11.
[4] Campbell JH, Suratwala TI. Nd-doped phosphate glasses for high-energy/high-peak-power lasers. J Non-Cryst Solids 2000;263 & 264:318–41.
[5] Sales BC, Boatmer LA. Lead-iron phosphate glass: a stable storage medium for high-level nuclear waste. Science 1984;226:45–8.
[6] Dimitrov V, Komatsu T. Electronic polarizability, optical basicity and non-linear optical properties of oxide glasses. J Non-Cryst Solids 1999;249:160–79.
[7] Boling N, Glass A, Owyoung A. Empirical relationships for predicting nonlinear refractive index changes in optical solids. IEEE J Quantum Electron 1978;QE-14:601–8.
[8] Ebendorff-Heiderpriem H, Ehrt D. Spectroscopic properties of Eu^{3+} and Tb^{3+} ions for local structure investigations of fluoride phosphate and phosphate glasses. J Non-Cryst Solids 1996;208:205–16.
[9] Karakassides MA, Saranti A, Koutselas I. Preparation and structural study of binary phosphate glasses with high calcium and/or magnesium content. J Non-Cryst Solids 2004;347:69–79.
[10] Cozar O, Magdas DA, Nasdala L, Ardelean I, Damian G. Raman spectroscopic study of some lead phosphate glasses with tungsten ions. J Non-Cryst Solids 2006;352:3121–5.
[11] Shih P. Properties and FTIR spectra of lead phosphate glasses for nuclear waste immobilization. Mater Chem Phys 2003;80:299–304.
[12] Gan FX. Optical and spectroscopic properties of glasses. Berlin/Heidelberg: Springer; 27.
[13] Henderson GS, Amos RT. The structure of alkali germanophosphate glasses by Raman spectroscopy. J Non-Cryst Solids 2003;328:1–19.
[14] Payne SA, Chase LL, Smith LK, Kway WL, Krupke WF. Infrared cross-section measurements for crystals doped with Er^{3+}, Tm^{3+} and Ho^{3+}. IEEE J Quantum Electron 1992;QE-28:2619–30.
[15] Gorller-Warland C, Binnimans K. In: Gschneidner Jr. KA, Eyring L, editors. Handbook on the physics and chemistry of rare earths, vol. 25. Amsterdam: North Holland; 1998 ([chapter 167]).
[16] McCumber DE. Einstein relations connecting broadband emission and absorption spectra. Phys Rev 1964;136:A954–7.
[17] Deloach LD, Payne SA, Chase LL, Smith LK, Kway WL, Krupke WF. Evaluation of absorption and emission properties of Yb^{3+} doped crystals for laser applications. IEEE J Quantum Electron 1993;24:1179–91.
[18] Patek K. Glass lasers. Butterworth; 1970.

[19] Carnall WT, Fields PR, Rajnak K. Spectral intensities of trivalent lanthanides and actinides in solution. II. J Chem Phys 1968;49:4412–23.
[20] Yeh DC, Sibley WA, Suscavage M, Drexhage MG. Radiation effects and optical transitions in Yb^{3+} doped barium–thorium fluoride glass. J Non-Cryst Solids 1986;88:66–82.
[21] Balaji S, Sontakke AD, Annapurna K. Yb^{3+} ion concentration effects on ~1 μm emission in tellurite glass. J Opt Soc Am B 2012;29:1569–79.
[22] Dai N, Hu L, Lu P. Effects of Yb ion concentration on the spectral properties of lead silica glasses. Opt Commun 2005;253:151–5.
[23] Barua P, Sekiya EH, Saito K, Ikushima AJ. Influences of Yb^{3+} ion concentration on the spectroscopic properties of silica glass. J Non-Cryst Solids 2008;354:4760–4.
[24] Feng X, Tanabe S, Handa T. Spectroscopic properties of erbium-doped ultraphosphate glasses for 1.5 μm amplification. J Appl Phys 2001;89:3560–7.
[25] Zhang L, Lu H. Evaluation of spectroscopic properties of Yb^{3+} in tetraphosphate glasses. J Non-Cryst Solids 2001;292:108–14.
[26] Sumida DS, Fan TY. Effect of radiation trapping on fluorescence lifetime and emission cross-section measurements in solid-state laser media. Opt Lett 1994;19:1343–5.
[27] Kassab LRP, Fukumoto ME, Cacho VDD, Wetter NU, Morimoto NI. Spectroscopic properties of Yb^{3+} doped $PbO–Bi_2O_3–Ga_2O_3$ glasses for IR laser applications. Opt Mater 2005;27:1576–82.
[28] Bell MJV, Quirino WG, Oliveira SL, de Sousa DF, Nunes LAO. Cooperative luminescence in Yb^{3+}-doped phosphate glasses. J Phys Condens Matter 2003;15:4877–87.
[29] Kassab LRP, Currol LC, Cacho VDD, Tatumi SH, Wetter NU, Gomes L, et al. $GeO_2–PbO–Bi_2O_3$ glasses doped with Yb^{3+} for laser applications. J Non-Cryst Solids 2004;348:103–7.
[30] Dai S, Yang J, Wen L, Hu L, Jiang Z. Effect of radiative trapping on measurement of the spectroscopic properties of Yb^{3+}:phosphate glasses. J Lumin 2003;104:55–63.
[31] Epstein RI, Buchwald MI, Edwards BC, Gosnell TR, Mungan CE. Observation of laser-induced fluorescent cooling of solids. Nature 1995;377:500–2.
[32] Auzel F. In: DiBartolo B, editor. Radiationless Processes. New Yark: Plenum Press; 1980. p. 213.
[33] Baldacchini G. In: DiBartolo B, editor. Advances in energy transfer processes. Singapore: World Scientific; 2001. p. 359.
[34] Auzel F. A fundamental self-generated quenching center for lanthanide-doped high-purity solids. J Lumin 2002;100:125–30.
[35] Choi JH, Margaryan A, Margaryan A, Shi FG. Spectroscopic properties of Yb^{3+} in heavy metal contained fluorophosphate glasses. Mater Res Bull 2005;40:2189–97.
[36] Choi JH, Margaryan A, Margaryan A, Shi FG. Optical transition properties of Yb^{3+} in new fluorophosphate glasses with high gain coefficient. J Alloys Compds 2005;396:79–85.
[37] Zhang Q, Ding J, Jang B, Cheng J, Qiao Y, Zhou Q, et al. Optical properties of Yb^{3+} ions in $SiO_2–Al_2O_3–CaF_2$ glasses. J Phys D Appl Phys 2009;42(235405):1–4.
[38] Petrov V, Griebner U, Ehrt D, Seeber W. Femtosecond self mode locking of Yb:fluoride phosphate glass laser. Opt Lett 1997;22:408–10.
[39] Zou X, Toratani H. Evaluation of spectroscopic properties of Yb^{3+}-doped glasses. Phys Rev B 1995;52:15889–97.
[40] Dai S, Hu L, Sugiyama A, Izawa Y, Zhuping L, Jiang Z. Study of a new ytterbium doped phosphate laser glass. Chin Sci Bull 2002;47:255–9.
[41] Venkata Krishnaiah K, Jayasankar CK, Venkatramu V, León-Luis SF, Lavín V, Chaurasia S, et al. Optical properties of Yb^{3+} ions in fluorophosphate glasses for 1.0 μm solid-state infra-red lasers. Appl Phys B 2013;113:527–35.
[42] Venkata Krishnaiah K, Jayasankar CK, Chaurasia S, Murali CG, Dhareshwar LJ. Preparation and characterization of Yb^{3+}-doped metaphosphate glasses for high energy and high power laser applications. Sci Adv Mater 2013;5:276–84.
[43] Jacinto C, Oliveira SL, Nunes LAO, Catunda T, Bell MJV. Thermal lens study of the OH^- influence on the fluorescence efficiency of Yb^{3+}-doped phosphate glasses. Appl Phys Lett 2005;86(071911):1–3.
[44] Auzel F, Goldner P. Towards rare-earth clustering in doped glasses. Opt Mater 2001;16:93–103.
[45] Chun J, Junzhou Z, Peizhen D, Cuosong H, Hanfen M, Gan F. Optimization of spectroscopic properties of ytterbium-doped laser glasses. Sci Chin (Ser E) 1999;42:616–22.
[46] Currol LC, Kassab LRP, Morais AS, Mendes CMS, Gomes L, Wetter NU, et al. Study of the most suitable new glass laser to incorporate ytterbium: alkali niobium tellurite, lead fluorborate or heavy metal oxide. J Lumin 2003;102–103:106–11.